

# Electrostatics in Periodic Slab Geometries II

Jason de Joannis,\* Axel Arnold,<sup>†</sup> and Christian Holm<sup>‡</sup>

Max-Planck-Institut für Polymerforschung, Ackermannweg 10, 55128 Mainz, Germany

(Dated: October 30, 2018)

In a previous paper a method was developed to subtract the interactions due to periodically replicated charges (or other long-range entities) in one spatial dimension. The method constitutes a generalized “electrostatic layer correction” (**ELC**) which adapts any standard 3D summation method to slab-like conditions. Here the implementation of the layer correction is considered in detail for the standard Ewald (**EW3DLC**) and the **P3M** mesh Ewald (**P3MLC**) methods. In particular this method offers a strong control on the accuracy and an improved computational complexity of  $O(N \log N)$  for mesh-based implementations. We derive anisotropic Ewald error formulas and give some fundamental guidelines for optimization. A demonstration of the accuracy, error formulas and computation times for typical systems is also presented.

## I. INTRODUCTION

Long-range forces, namely gravitation and electromagnetic interactions, are difficult to treat exactly in many-particle systems. In condensed matter, biological and solid state physics, there is considerable interest in the simulation of charged and polar molecules embedded in a slab in which the particles are replicated periodically in two directions. The applications range widely to include soap bubbles, cell membranes and electrochemistry. Surprisingly Ewald and other rapidly convergent methods for computing long-range interactions in infinitely periodic systems are computationally more demanding when the system is periodic in only one or two of the three spatial dimensions because of the breaking of spatial symmetry.

Several “two-dimensional Ewald” (**EW2D**) methods have already been proposed<sup>1</sup>. The most successful is that introduced by Parry<sup>2,3</sup> and others<sup>4,5</sup>. This method can be used to obtain accurate results but is limited to small systems (i.e.  $10^2$  to  $10^3$  charges). This springs from the fact that the pair separations,  $\mathbf{r}_{ij}$ , are no longer separable in the Fourier summation because of the necessary decoupling of the aperiodic  $z$  component from the periodic  $x$  and  $y$  components. Therefore it appears that the complexity (scaling of time with number of charges) of this method can be no better than quadratic. Also the one dimensional Ewald method<sup>6</sup> suffers from the same problem.

A promising alternative to Ewald summation is possible using a convergence-factor technique<sup>7</sup>. The basic Coulomb pair interaction is multiplied by one with the factor  $\lim_{\beta \rightarrow \infty} e^{-\beta r_{ijn}}$ . It is crucial to prove that the limit can be taken outside of the summation and now the modified potential is more readily susceptible to analysis. In a recent study,<sup>8</sup> Arnold and Holm derive a two-dimensional version of this method with complexity  $N^{5/3}$  along with accurate error formulas. This method is particularly attractive when extremely high accuracy is desired. We will use this method, abbreviated as **MMM2D** and the **EW2D** algorithm mentioned above as reference methods.

One idea, used several times to study water interfaces, introduces a spatial constraint within the simulation cell. If the box has dimensions  $L_x \times L_y \times L_z$ , the particles may have  $z$ -coordinates on  $[0, h)$ , while the space within  $[h, L_z)$  (the gap size) remains empty<sup>9</sup>. The primary cell is, as usual, replicated in all three directions periodically. The effect of this is to create a “primary layer” and an empty layer followed by an infinite array of intercalated image and empty layers. Figure 1 summarizes the essential geometrical considerations in this problem. While this idea seems trivially to be correct, it has one flaw. The flaw can be realized by attempting to reproduce the results of an **EW2D** calculation using a three dimensional Ewald summation (**EW3D**) as just described. One will find that the results always differ by a dipole-moment dependent constant. This fact, although at first thought to be merely a slow convergence issue, was noticed by Spohr<sup>10</sup>. The **EW3D** formula contains a shape dependent dipole-term whose origin was mathematically proven in the 1980’s<sup>11,12</sup>, that reflects the naturally chosen spherical order of summation in the conditionally convergent Coulomb sum. For the case of layers, however, it is necessary to use a *slab-wise summation order*. This was realized by Yeh and Berkowitz<sup>13</sup>, who applied a theory due to E. R. Smith<sup>14</sup> for infinite crystals of various shapes in order to obtain the correct dipole term for a slab-wise summation order. Another complication arises, if the periodic supersystem is surrounded by some medium with a different dielectric constant. This medium has a polarizing effect on the particles in the simulation cell no matter how large the supersystem is. For the remainder of this paper we consider only the simple case of zero contrast for which the dielectric constant is the same inside and outside the supersystem. This is often referred to as the vacuum boundary condition.

One of the advantages of using this method from a practical point of view is that any standard Ewald program may be used with only minor modification. It is easy to show numerically that the use of this new dipole term and sufficient spacing ( $L_z - h$ ), yields the same result as two-dimensional “brute force”, **MMM2D** and **EW2D** summation methods. As explained in a previous paper, referred to here as “paper I”<sup>15</sup>, errors introduced due to the

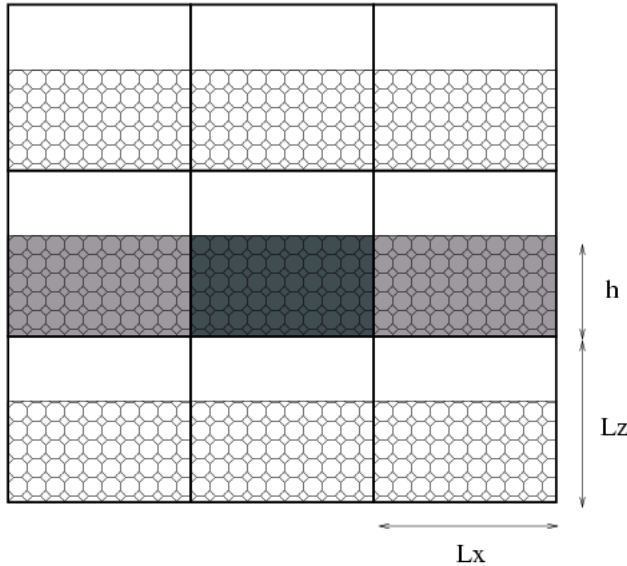


FIG. 1: Schematic of periodicity.

TABLE I: Methods for slab geometry.

method	authors	complexity
<b>EW2D</b>	Parry; HBC; DP <sup>2,4,5</sup>	$N^2$
<b>Lekner</b>	Lekner <sup>18</sup>	$N^2$
<b>MMM2D</b>	Arnold & Holm <sup>8</sup>	$N^{5/3}$
<b>EW3DC</b>	Yeh & Berkowitz <sup>13</sup>	$N^{3/2}$
<b>EW3DLC</b>	Ewald <sup>19</sup> + <b>ELC</b>	$N^{3/2}$
<b>P3MLC</b>	Hockney & Eastwood <sup>20</sup> + <b>ELC</b>	$N \log N$
<b>MMMLC</b>	Sperb & Strelbel <sup>7</sup> + <b>ELC</b>	$N \log N$
<b>FMMLC</b>	Greengard & Rhoklin <sup>16</sup> + <b>ELC</b>	$N$

image layer effects decay exponentially with the size of the gap. This method is sometimes referred to as a corrected three-dimensional Ewald sum (**EW3DC**)<sup>13</sup>. Like the original Ewald method it has a complexity of  $N^{3/2}$  and the equations can be discretized onto a mesh yielding an  $N(\log N)^{3/2}$  complexity. In paper I<sup>15</sup>, we derived an analytic electrostatic layer correction term, called **ELC**-term, that subtracts the interactions of the unwanted slab replicas. This term can be evaluated linearly in  $N$ , and has full error control. The use of the **ELC** term and the change of summation order, shortly called the **ELC** method, enables us to adapt any 3D summation method, such as the non-Ewald convergence-factor<sup>7</sup> and multipole expansion<sup>16</sup> methods, to slab geometries. The latter of these, though in possession of a slightly better scaling, has such a considerable amount of overhead that it is useful only for much larger systems than normally used<sup>17</sup>. The abbreviations and complexities of some of the two-dimensional methods available at present are summarized in Table I, where the ending LC always denotes the use of the **ELC** method. In this terminology the **EW3D** algorithm plus the **ELC** method is called **EW3DLC** and so on.

This paper is organized as follows. In Sec. II the equations required for implementation of **EW3DLC** are collected and discussed. In Sec. III the standard Ewald error formulas are extended for anisotropic systems and the error formula for the new layer correction term is described. The methodology is demonstrated on several test-systems in

Sec. IV and the efficiency compared with other 2D methods is shown in Sec. V. Finally the results of this paper and the outlook for computational studies of slab geometries are summarized in Sec. VI. In the Appendix we give explicit formulas for the **ELC**-term contributions to the force and the diagonal part of the stress tensor.

## II. EW3DLC IN A NUTSHELL

The electrostatic energy of one section of a periodic slab follows from the classical formula for the Coulomb pair potential. Omitting the prefactor  $(1/4\pi\epsilon_0)$ ,

$$E = \frac{1}{2} \sum'_{\mathbf{n}_\parallel} \sum_{i,j=1}^N \frac{q_i q_j}{|\mathbf{r}_{ij} + \mathbf{n}_\parallel|}. \quad (1)$$

This serves as a useful point of introduction to our notation:  $N$  particles with charges  $q_i$  and positions  $\mathbf{r}_i$ , reside in a simulation box of edges  $L_x \times L_y \times L_z$ . The image boxes are denoted using the vector  $\mathbf{n}_\parallel \in (\mathbb{Z}L_x, \mathbb{Z}L_y, 0)$  and  $\mathbf{r}_{ij} = \mathbf{r}_i - \mathbf{r}_j$ . The prime on the inner summation indicates the omission of the primary box,  $\mathbf{n}_\parallel = (0, 0, 0)$ , when  $i = j$  (the singular case). Strictly speaking the sum over  $\mathbf{n}_\parallel$  is ill-defined without specification of the order of summation. This is a consequence of the fact that summations of the type  $|\mathbf{n} + c|^{-\xi}$  are conditionally convergent for  $0 < \xi < d$ , where  $d$  is the dimensional periodicity. The summation limit of relevance is an expanding cylinder or disc such that the summation terms appear in order of increasing  $|\mathbf{n}_\parallel|$ .

We convert this into a three-dimensional problem by nesting the  $L_x \times L_y \times h$  particle volume within a larger  $L_x \times L_y \times L_z$  box, thereby creating a screen for the ghost charges (the new image charges) as described in the introduction. The total electrostatic energy  $E$  is, via combination of the celebrated Ewald identity and the recent convergence-parameter layer correction, rewritten in the computationally convenient form:

$$E = E^{(r)} + E^{(k)} + E^{(s)} + E^{(d)} + E^{(lc)}, \quad (2)$$

where the individual terms are as follows,

$$E^{(r)} = \frac{1}{2} \sum_{i,j=1}^N \sum'_{\mathbf{n}} q_i q_j \frac{\operatorname{erfc}(\alpha |\mathbf{r}_{ij} + \mathbf{n}|)}{|\mathbf{r}_{ij} + \mathbf{n}|} \quad (3)$$

$$E^{(k)} = \frac{1}{2} \frac{1}{L_x L_y L_z} \sum_{\mathbf{k} \neq 0} \frac{4\pi}{k^2} e^{-k^2/4\alpha^2} \left| \sum_{j=1}^N q_j e^{i\mathbf{k} \cdot \mathbf{r}_j} \right|^2 \quad (4)$$

$$E^{(s)} = -\frac{\alpha}{\sqrt{\pi}} \sum_i q_i^2 \quad (5)$$

$$E^{(d)} = \frac{2\pi}{L_x L_y L_z} \left( \sum_i q_i z_i \right)^2 \quad (6)$$

$$\begin{aligned} E^{(lc)} = & -\frac{8\pi}{L_x L_y} \sum_{k_x, k_y > 0} \frac{1}{k_\parallel (e^{k_\parallel L_z} - 1)} \sum_{p,q,r=1}^2 (-1)^p \chi_{pqr}^2 \\ & -\frac{4\pi}{L_x L_y} \sum_{k_x > 0} \frac{1}{k_x (e^{k_x L_z} - 1)} \sum_{p,q=1}^2 (-1)^p \chi_{pq0}^2 \\ & -\frac{4\pi}{L_x L_y} \sum_{k_y > 0} \frac{1}{k_y (e^{k_y L_z} - 1)} \sum_{p,q=1}^2 (-1)^p \chi_{p0q}^2 \end{aligned} \quad (7)$$

where the summations run over  $\mathbf{n} \in (\mathbb{Z}L_x, \mathbb{Z}L_y, \mathbb{Z}L_z)$  and  $\mathbf{k} \in 2\pi(\mathbb{Z}/L_x, \mathbb{Z}/L_y, \mathbb{Z}/L_z)$  and are order-independent. As usual, the symbol  $\alpha$  denotes the Ewald parameter which: (1) determines the radius of the Gaussian charge distributions, (2) has units of inverse length and (3) can take any value without changing the net result for the energy, but has an optimum with respect to convergence of the summations. The first three terms (Eqs. 3–5) correspond to the usual Ewald real (r), Fourier (k) and self (s) contributions to the energy. The dipole term  $E^{(d)}$  arises from the cylindrical or slab-wise summation limit as discussed in paper I<sup>15</sup> and at length in the introduction. It differs from the spherical version by a factor of 3 and by the replacement of the total dipole moment with its  $z$ -component. Again,

this dipole term applies only to vacuum boundary conditions. The final term  $E^{(lc)}$  is the energy subtraction due to all image layers. This term was derived in paper I and is shown here in an expanded  $O(N)$  form. These summations run over the variables  $k_x, k_y \in 2\pi\mathbb{Z}/L_x, 2\pi\mathbb{Z}/L_y$  and the parallel combination of these is  $k_{\parallel} = \sqrt{k_x^2 + k_y^2}$ . The component abbreviations are as follows,

$$\chi_{1/2,1/2,1/2} = \sum_{i=1}^N q_i \sinh / \cosh(k_{\parallel} z_i) \sin / \cos(k_x x_i) \sin / \cos(k_y y_i) \quad (8)$$

and a subscript of zero stipulates omission of the corresponding trigonometric function. For example,  $\chi_{2,0,1} = \sum q_i \cosh(k_{\parallel} z_i) \sin(k_y y_i)$ . The corresponding equations for the forces can be obtained by differentiation of Eqs. 3–7, i.e.  $\mathbf{f}_i = -\nabla_i E$ .

The derivation of the layer correction energy is a crucial part of the method so we shall recapitulate it here in brief. The objective is to obtain a rapidly convergent linear expression for the total energy of interaction of the particles in the primary box with the ghost charges:

$$E^{(lc)} = -\frac{1}{2} \sum_{n_z \neq 0} \sum_{\mathbf{n}_{\parallel}} \sum_{i,j=1}^N \frac{q_i q_j}{|\mathbf{r}_{ij} + \mathbf{n}_{\parallel}|}. \quad (9)$$

It is quite similar in appearance to the original formula (Eq. 1), and can be treated analogously by convergence factors as in the study by Arnold and Holm<sup>8</sup>.

We have not here written explicitly the summation order but nevertheless this is an important consideration.<sup>21</sup> With the Poisson summation formula applied along each periodic direction a transformation of the in-plane variables,  $n_x$  and  $n_y$ , into Fourier conjugates  $k_x$  and  $k_y$  is achieved. The derivation depends heavily on the requirement that the system is overall neutral and results finally in

$$E^{(lc)} = - \sum_{i,j=1}^N q_i q_j \left( \begin{aligned} & \frac{8\pi}{L_x L_y} \sum_{k_x, k_y > 0} \frac{\cosh(k_{\parallel} z_{ij})}{k_{\parallel}(e^{k_{\parallel} L_z} - 1)} \cos(k_x x_{ij}) \cos(k_y y_{ij}) + \\ & \frac{4\pi}{L_x L_y} \sum_{k_x > 0} \frac{\cosh(k_x z_{ij}) \cos(k_x x_{ij})}{k_x(e^{k_x L_z} - 1)} + \\ & \frac{4\pi}{L_y L_x} \sum_{k_y > 0} \frac{\cosh(k_y z_{ij}) \cos(k_y y_{ij})}{k_y(e^{k_y L_z} - 1)} \end{aligned} \right). \quad (10)$$

It is fortunate (in contrast to **EW2D**) that the coordinates appear as they do because after decomposition of the  $\cos$  and  $\cosh$  terms, the  $N^2$  summation collapses, yielding the order  $N$  Eq. 7. For reference purposes we have assembled in the appendix the full expressions for the force and the diagonal parts of the stress tensor due to the **ELC**-term.

### III. ERROR ESTIMATES

The most important measures of error in an electrostatic calculation are the root mean squared error in the particle forces,

$$\Delta f := \left( \frac{1}{N} \sum_{i=1}^N \Delta \mathbf{f}_i^2 \right)^{1/2}, \quad (11)$$

where  $\Delta \mathbf{f}_i$  is the difference between the computed and exact force on particle  $i$ , and the absolute value of the error in the total electrostatic energy,  $\Delta E$ . We will discuss mainly the former, which is relevant to molecular dynamics simulations.

The total error can be separated into terms originating from the cutoffs used for the Ewald and layer correction,

$$\Delta f \cong \sqrt{\Delta f_r^2 + \Delta f_k^2 + \Delta f_l^2}, \quad (12)$$

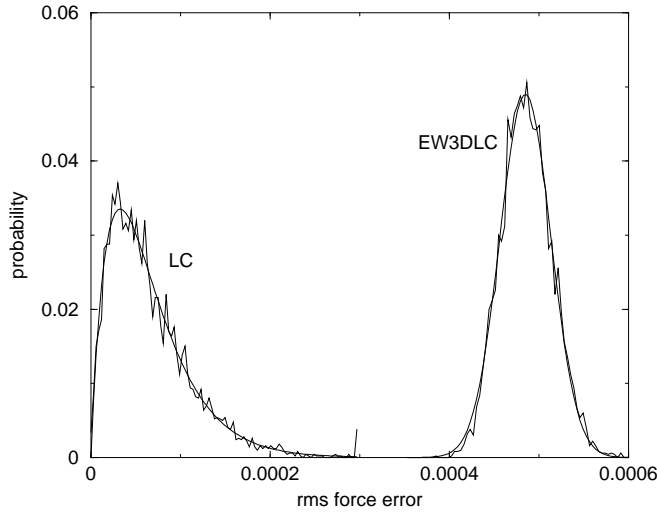


FIG. 2: Error distributions for **EW3DLC**,  $p(\Delta f)$ , and layer correction ,  $p(\Delta f_{lc})$ , for a 100 particle system of physical dimensions  $1.0 \times 1.0 \times 0.9$ . Convergence parameters for **EW3DLC**:  $\alpha = 9.3$ ,  $r_c = 0.36$ ,  $k_c = 10$ ,  $L_z = 2.0$ ,  $\Delta f_{lc} < 10^{-3}$ ; for LC:  $L_z = 1.0$ ,  $\Delta f_{lc} < 10^{-2}$ .

where the individual components are determined in the same way as in Eq. 11. Analytical error estimates for the real- and reciprocal-space terms for a cubic simulation box have been previously derived.<sup>22,23</sup> Shortly we will extend these results to obtain the formulas for arbitrary box sizes, but we write first the result,

$$\Delta f_r(\alpha, r_c) = \frac{2}{\sqrt{L_x L_y L_z}} \frac{Q^2}{\sqrt{N}} \frac{\exp[-\alpha^2 r_c^2]}{\sqrt{r_c}}, \quad (13)$$

$$\Delta f_k(\alpha, k_c) = \frac{2\alpha}{\sqrt{\pi L_y L_z}} \frac{Q^2}{\sqrt{N}} \frac{\exp[-(\pi k_c / \alpha L_x)^2]}{\sqrt{k_c}}, \quad (14)$$

where  $Q^2 = \sum_{i=1,N} q_i^2$ ,  $r_c$  is the real-space minimum image cutoff (typically but not necessarily  $\leq \frac{1}{2} \min[L_x, L_y, L_z]$ ) and  $k_c$  is an integer defining the truncation of the reciprocal-space summation. These naturally reduce to the standard formulas when the box is cubic. The optimum set of convergence parameters is obtained by setting  $\Delta f_r^2 = \Delta f_k^2$ . This reduces the number of independent variables to one yielding implicit relations  $\alpha(k_c)$ ,  $r_c(k_c)$ . Then one can easily scan  $k_c$  to find the optimum (i.e. fastest)  $k_c^*$ .

If the reciprocal space computation is instead handled by FFT methods such as **P3M**, inaccuracies arise due to the assignment and de-assignment of the charges onto a mesh. The error for **P3M** has been estimated (for a cubic system) by

$$\Delta f_{P3M}(\alpha, M, P) = \frac{Q^2}{L^2 \sqrt{N}} \left( \frac{\alpha L}{M} \right)^P \sqrt{\alpha L \sqrt{2\pi} \sum_{k=0}^{P-1} a_k^{(P)} \left( \frac{\alpha L}{M} \right)^{2k}} \quad (15)$$

where  $M$  is the number of mesh points per edge and  $P$  is the interpolation order. The expansion coefficients,  $a_k^{(P)}$  are constants given by Deserno and Holm.<sup>24</sup> A more accurate numerical error estimate is also given by these authors but Eq. 15 is useful since it captures the function form of the error.

The Ewald terms have the advantage of well-behaved error distributions. This is not the case when turning to the layer correction term. Consider for example the probability distribution of  $\Delta f$  and  $\Delta f_{lc}$  over the ensemble of random particle configurations as shown in Fig. 2. The former distribution was generated under conditions of negligible layer correction error while the latter distribution is for layer correction error itself under conditions where it is significant (i.e. small gap). The distribution of the total **EW3DLC** error fits very well to a Gaussian curve. The error distribution of the layer correction term on the other hand is skewed to the left and fits well to a stretched exponential  $p(x) \propto x \exp(-ax)$ . The extended tail of this distribution means that exceptions to the average error will occur with non-negligible frequency. This feature makes it difficult to derive an accurate RMS error estimate for the

layer correction. But what is possible and more useful is the derivation of a stricter error criterion, namely an upper bound on the RMS error. A rigorous upper bound was derived in the first paper yielding,

$$\begin{aligned} \Delta f_{lc}(l_c, L_z) \leq & \frac{Q^2}{\sqrt{N}} \frac{\sqrt{3}}{2(e^{2\pi l_c L_z / L} - 1)} \left( \left( \frac{2\pi l_c + 4}{L} + \frac{1}{L_z - h} \right) \frac{e^{2\pi l_c h / L}}{L_z - h} \right. \\ & \left. + \left( \frac{2\pi l_c + 4}{L} + \frac{1}{L_z + h} \right) \frac{e^{-2\pi l_c h / L}}{L_z + h} \right), \end{aligned} \quad (16)$$

where  $l_c$  is the integer-valued radial cutoff for truncation of the layer correction forces.

Before leaving this topic a reminder is due of the bias present in slab geometries. Both the Ewald and layer correction terms have an error bias with respect to the  $z$ -position of a particle. The error tends to be higher near the walls of the system as if it were “hotter” in those regions. In fact, one can imagine a simulation in which the overall RMS error in the forces is smaller than the RMS random force but due to this bias, the RMS force-error at the surfaces is larger than the thermal noise, amounting to true hot zones at the surfaces. Therefore it is recommended to exercise some caution in the treatment of these effects. The layer correction error in particular has a strong surface bias, and it is therefore quite appropriate to use an upper bound in place of an RMS error estimate. In other words, the layer correction should be carried out to higher accuracy than the real and reciprocal space parts.

### Anisotropic Real-Space Error

Let us write down the real-space force first,

$$\mathbf{f}_i^{(r)} = \sum_{j=1}^N q_i q_j \sum'_{\mathbf{n}} \mathbf{r}_{ijn} \left[ \frac{2\alpha}{\sqrt{\pi}} \frac{e^{-\alpha^2 r_{ijn}^2}}{r_{ijn}^2} + \frac{\text{erfc}(\alpha |\mathbf{r}_{ijn}|)}{|\mathbf{r}_{ijn}| r_{ijn}^2} \right]. \quad (17)$$

This is always summed using a minimum image spherical cutoff  $|r_{mijn}| < r_c$  regardless of the system geometry. Therefore the error in truncation of Eq. 17 for the force on particle  $i$  is

$$\delta \mathbf{f}_i = q_i \sum_{j=1}^N \sum_{\mathbf{n}: |\mathbf{r}_{ijn}| > r_c} q_j \mathbf{r}_{ijn} g(|\mathbf{r}_{ijn}|), \quad (18)$$

where  $g$  is an abbreviation for the term in square brackets. We square this and obtain

$$(\delta \mathbf{f}_i)^2 = q_i^2 \sum_{j \neq k} q_j q_k \sum_{|\mathbf{r}_1| > r_c} \sum_{|\mathbf{r}_2| > r_c} \mathbf{r}_1 \cdot \mathbf{r}_2 g(|\mathbf{r}_1|) g(|\mathbf{r}_2|) + q_i^2 \sum_{j=1}^N q_j^2 \sum_{\mathbf{n}: |\mathbf{r}_1| > r_c} \mathbf{r}_1^2 g^2(|\mathbf{r}_1|), \quad (19)$$

where  $\mathbf{r}_1, \mathbf{r}_2$  are the vectors pointing from particle  $i$  to the  $n^{th}$  images of  $j$  and  $k$  respectively. Since  $g$  is an even function and  $q_1, q_2$  will take negative and positive values the average of this quantity over all the  $i$  particles in the system contains, in the limit of large, uncorrelated  $N$ , only the diagonal terms. Thus

$$\langle (\delta \mathbf{f}_i)^2 \rangle = q_i^2 \sum_{j=1}^N q_j^2 \sum_{n: |\mathbf{r}_1| > r_c} \mathbf{r}_1^2 g^2(|\mathbf{r}_1|). \quad (20)$$

Moreover in the statistical limit the summation  $\Sigma_n$  is independent of particles  $i$  and  $j$  and we have

$$\langle (\delta \mathbf{f}_i)^2 \rangle^{1/2} = |q_i| Q \Sigma_n^{1/2}, \quad (21)$$

where  $Q^2 = \sum q_j^2$ . We will proceed by treating the summation as a spherical integral. First we write the variable explicitly

$$|\mathbf{r}_1| = \sqrt{(x + sL_x)^2 + (y + tL_y)^2 + (z + uL_z)^2} = \rho \quad (22)$$

where  $s, t, u \in \mathbb{Z}$ . In Cartesian coordinates we have the following integration

$$\Sigma_n \approx \frac{8}{L_x L_y L_z} \int_{\tilde{c}_s}^{\infty} d\tilde{s} \int_{\tilde{c}_t}^{\infty} d\tilde{t} \int_{\tilde{c}_u}^{\infty} d\tilde{u} \rho^2 g^2(\rho) = \frac{4\pi}{L L_y L_z} \int_{r_c}^{\infty} d\rho \rho^4 g^2(\rho) \quad (23)$$

where we have applied  $\tilde{s} = s/L_x$  etc.

The final step involves the application of the asymptotic integral expansion,

$$\int_z^\infty f(x)e^{-ax^2} dx \approx \frac{f(z)e^{-az^2}}{2az} \quad (24)$$

where the validity of this relation is discussed by Kolafa & Perram. We can apply this formula twice to obtain our mean-squared particle error;

$$\operatorname{erfc}(\alpha\rho) \approx \frac{e^{-\alpha^2\rho^2}}{2\alpha\rho} \quad (25)$$

and

$$\int_c^\infty d\rho e^{-2\alpha^2\rho^2} \left[ \frac{2\alpha}{\sqrt{\pi}} + \frac{1}{2\alpha\rho^2} \right]^2 \approx \left( \frac{1}{\sqrt{\pi r_c}} + \frac{1}{4\alpha^2 r_c^{5/2}} \right)^2 e^{-2\alpha^2 r_c^2}. \quad (26)$$

Finally we can obtain the root mean squared force error,

$$\Delta f = \sqrt{N^{-1} \sum_{m=1}^N \delta f_m} \approx \frac{Q}{\sqrt{N}} \left( \frac{\langle (\delta f_m)^2 \rangle}{q_m^2} \right)^{1/2} = \frac{2Q^2}{\sqrt{N}} \frac{1}{\sqrt{L_x L_y L_z}} \left( \frac{1}{\sqrt{r_c}} + \frac{\sqrt{\pi}}{4\alpha^2 r_c^{5/2}} \right) e^{-\alpha^2 r_c^2}. \quad (27)$$

Neglecting the smaller  $\alpha^{-2}$  term yields Eq. 13.

### Anisotropic Reciprocal-Space Error

First we write the generalized anisotropic  $k$ -space force on particle  $i$ ,

$$\mathbf{f}_i^{(k)} = \frac{q_i}{L_x L_y L_z} \sum_j q_j \sum_{\mathbf{k} \neq 0} \frac{4\pi\mathbf{k}}{k^2} \exp\left(-\frac{k^2}{4\alpha^2}\right) \sin(\mathbf{k} \cdot \mathbf{r}_{ij}), \quad (28)$$

where again  $\mathbf{k} \in 2\pi(\mathbb{Z}/L_x, \mathbb{Z}/L_y, \mathbb{Z}/L_z)$ .

The summation will be approximated using a cutoff  $\tau$  and therefore only terms satisfying

$$\mathbf{k}^2 \leq \tau^2 \quad (29)$$

will be added. This equation defines the interior of an ellipsoid whose axes are  $L_x/2\pi$ , etc.

Now we compose the cutoff error for a single pair of particles, for which it will prove useful to write using complex notation. Using the fact the function in front of the sin is odd and that half of the vectors  $\mathbf{k}$  are identical but opposite in sign to the other half we obtain

$$\delta \mathbf{f}_{ij} = -\frac{q_i q_j}{L_x L_y L_z} \sum_{|\mathbf{k}| > \tau} \frac{4\pi\mathbf{k}}{k^2} \exp\left(-\frac{k^2}{4\alpha^2}\right) i \exp(i\mathbf{k} \cdot \mathbf{r}_{ij}). \quad (30)$$

Taking the square of this yields

$$(\delta \mathbf{f}_{ij})^2 = - \left( \frac{q_i q_j}{L_x L_y L_z} \right)^2 \sum_{|\mathbf{k}_1| > \tau} \sum_{|\mathbf{k}_2| > \tau} \frac{16\pi^2 \mathbf{k}_1 \cdot \mathbf{k}_2}{k_1^2 k_2^2} e^{-(k_1^2 + k_2^2)/4\alpha^2} \exp(i\mathbf{k}_1 \cdot \mathbf{r}_{ij}) \exp(i\mathbf{k}_2 \cdot \mathbf{r}_{ij}). \quad (31)$$

At this point we remind ourselves that, in spite of how it looks, this expression is indeed real and positive-valued. We want to obtain the average of this function over all the particle pairs in the system. In the limit of many uncorrelated particles the following expression is exact,

$$\langle \exp(i\mathbf{k}_1 \cdot \mathbf{r}_{ij}) \exp(i\mathbf{k}_2 \cdot \mathbf{r}_{ij}) \rangle_{ij} = \delta(\mathbf{k}_1, -\mathbf{k}_2). \quad (32)$$

The details of this require the observation that  $\langle s_1 c_2 \rangle = \langle s_1 s_2 \rangle = \langle c_1 c_2 \rangle = 0$  for  $\mathbf{k}_1 \neq \mathbf{k}_2, \neq -\mathbf{k}_2$  and  $\langle s^2 \rangle = \langle c^2 \rangle$  where the abbreviations  $s_1 = \sin(\mathbf{k}_1 \cdot \mathbf{r}_{ij})$  and  $c_1 = \cos(\mathbf{k}_1 \cdot \mathbf{r}_{ij})$  have been used. Finally we reach a greatly simplified version of the root-mean-squared pair-wise error:

$$\langle (\delta \mathbf{f}_{ij})^2 \rangle^{1/2} = \frac{|q_i||q_j|}{L_x L_y L_z} \left( \sum_{|\mathbf{k}| > \tau} \frac{16\pi^2}{k^2} e^{-k^2/2\alpha^2} \right)^{1/2}. \quad (33)$$

Now we will be somewhat explicit in treating the summation above. We rewrite the summation in terms of its fundamental variables and length scales,

$$\sum_{|\mathbf{k}| > \tau} \frac{e^{-k^2/2\alpha^2}}{k^2} = \frac{L_x^2}{4\pi^2} \sum_{\rho^2 > k_c^2} \frac{\exp[-a\rho^2]}{\rho^2}. \quad (34)$$

Here we are taking  $a = 2\pi^2/\tilde{\alpha}^2 = 2\pi^2/(\alpha L)^2$ ,  $\lambda = L_x/L_z$ ,  $\gamma = L_x/L_y$ ,  $\rho^2 = l^2 + m^2\gamma^2 + n^2\lambda^2$ ,  $l, m, n \in \mathbb{Z}$  and  $k_c$  is the integer cutoff which defines an ellipsoidal solid upon  $\mathbb{Z}^3$ . With this notation, all of the units of the expression are carried by the factor  $L_x^2$ . This equation can be approximated by integration; in Cartesian coordinates

$$\approx 8 \frac{L_x^2}{4\pi^2} \int_{S1} dl \int_{S2} dm \int_{S3} dn \frac{\exp[-a(l^2 + m^2\gamma^2 + n^2\lambda^2)]}{l^2 + m^2\gamma^2 + n^2\lambda^2}, \quad (35)$$

where the limits which we do not write here, will collapse into a much simpler form. Conversion to spherical coordinates requires only the substitutions  $\tilde{n} = \lambda n$ ,  $\tilde{m} = \gamma m$  and we have

$$\frac{L_x^2}{\pi} \gamma^{-1} \lambda^{-1} \int_{k_c}^{\infty} \rho^2 d\rho \frac{\exp(-a\rho^2)}{\rho^2} \approx \frac{L_x^2}{\pi} \gamma^{-1} \lambda^{-1} \frac{\exp(-ak_c^2)}{2ak_c}. \quad (36)$$

To summarize the results of this section, we have found

$$\sum_{|\mathbf{k}| > \tau} \frac{e^{-k^2/2\alpha^2}}{k^2} \approx L^2 \frac{\tilde{\alpha}^2}{4\pi^3 \gamma \lambda l_c} \exp(-2\pi^2 k_c^2/\tilde{\alpha}^2), \quad (37)$$

a result that was obtained by imposing a single-parameter ellipsoidal cutoff which makes simple spherical integration possible. That is to say, if we had not restricted the degrees of freedom of the cutoff object, then we would be faced with the daunting task of ellipsoidal integration. Two assumptions were made, namely that the function varies slowly enough across the grid points so that integration is valid, and secondly that the integral theorem mentioned by Kolafa & Perram is accurate.

We can write the RMS error, first we have the pair-wise error approximated as

$$\langle (\delta \mathbf{f}_{ij})^2 \rangle^{1/2} = \frac{|q_i||q_j|}{L_y L_z} \frac{2}{\sqrt{\pi}} \frac{\tilde{\alpha}}{\sqrt{\gamma \lambda k_c}} \exp(-\pi^2 k_c^2/\tilde{\alpha}^2); \quad (38)$$

which leads to

$$\Delta f \approx \sqrt{\frac{1}{N} \sum_{i=1}^N \sum_{j \neq i} \langle (\delta \mathbf{f}_{ij})^2 \rangle} \approx \frac{Q^2}{\sqrt{N}} \frac{2}{\sqrt{\pi}} \frac{1}{L_y L_z} \frac{\tilde{\alpha}}{\sqrt{\gamma \lambda k_c}} \exp(-\pi^2 k_c^2/\tilde{\alpha}^2). \quad (39)$$

#### IV. DEMONSTRATION OF ACCURACY

In this section we demonstrate the credibility of the **EW3DLC** technique by means of several standardized test cases that have been used in other literature. These fall into two categories: (1) two-particle systems and (2) a single charge elevated above a planar array of 25 charges. These cases are known to emphasize the possible errors arising from the non-periodicity in the  $z$ -direction. Secondly, several tests of the error formulas are carried out to see that they are indeed applicable to non-cubic, inhomogeneous systems. For these tests it is sufficient to use a standard three-dimensional Ewald summation.

In Fig. 3 the results from a two-particle system are given. In this system the first particle is fixed and the second particle is moving in the  $z$  direction. For the remainder of this paper we will use  $L_x = L_y = L$  and unless otherwise

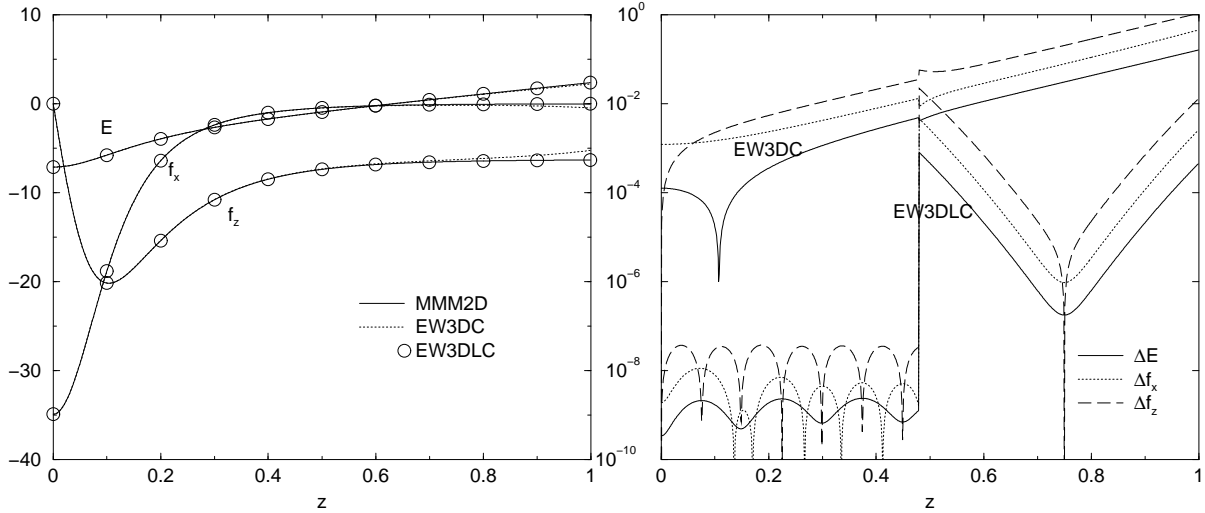


FIG. 3: Energy and force in a two-particle system:  $\mathbf{r}_1 = (0, 0, 0)$ ,  $\mathbf{r}_2 = (0.1, 0.1, z)$ ,  $q_1 = -1$  and  $q_2 = 1$ . As a reference, a well-converged ( $\Delta f < 10^{-10}$ ) **MMM2D** calculation is used. Convergence parameters:  $\alpha = 5.0$ ,  $k_c = 10$ ,  $r_c = 0.5$ ,  $L_z = 1.5$ ,  $\Delta f_{lc} < 10^{-10}$ . (a) Energy and forces. (b) Absolute error in energy and forces.

noted  $L$  is set equal to unity. In principle there is no limitation on the accuracy of the **EW3DLC** or **EW3DC** methods. The only visible errors (Fig. 3a) occur for the **EW3DC** method as  $z \rightarrow 1$  since the particle begins to approach the nearest image layer. This error can be eliminated (at some computational cost) by increasing  $L_z$ , but we are interested in illustrating the point.

A richer picture is obtained by plotting the errors on a semi-log scale (Fig. 3b). The **EW3DLC** curves are complex but these quirks vanish already in 3 or 4 particle systems and are more a signature of the underlying features of the Ewald equations. The key to the explanation of these features is the spherical minimum image cutoff which we chose as  $r_c = 0.5$ . When  $z$  reaches 0.48, the particles are no longer in view of each other, nor are any of the images in view. This leads on the right side of the plot to a significant underestimate of the real-space energy and force and is dominated by the exponential in Eq. 3. The left half of the **EW3DLC** curves are dominated by Fourier-space error which is trigonometric with a period of  $(k_c + 1)L/L_z$  due to the complex exponential in Eq. 4. Thus the final conclusion is that the basic two-particle curves exhibit nothing problematic in terms of the force and energy signatures.

The next test-system is the 26-particle one originally used by Widmann and Adolf<sup>1</sup>: a square array of 25 particles in the  $z = 0$  plane with coordinates  $(x, y, 0)$  where  $x, y \in (0.1, 0.3, 0.5, 0.7, 0.9)$ , and the 26th particle hovers above the center at  $(0.5, 0.5, 0.2)$ . The values reported previously are easily reproduced using a layer correction. For example, setting  $(\alpha, r_c, k_c, L_z) = (15.0, 0.40, 15, 0.80)$  produces  $-86.5655$  and  $-10.3642$  for the total energy and the  $z$ -component force of the 26th particle respectively. For the layer correction the the maximal pairwise error was set at  $10^{-6}$ . The layer correction contribution in this case is important even though the box edge is four times the layer thickness, amounting to  $-0.178234$  and  $0.476241$  for the force and energy respectively.

With these basic properties of the proposed algorithm established we may begin to probe its applicability to realistic systems. To this end we generate a “random” system of 100 unit charges (overall electrically neutral). We have followed the same convention as Ref.<sup>25</sup> so that these systems can be reproduced by other researchers. A set of 300 random numbers  $n_1, n_2, \dots, n_{300}$  between 0 and 1 and the coordinates of the charges are taken as  $\mathbf{r}_1 = (n_1 L, n_2 L, n_3 L_z)$ ,  $\mathbf{r}_2 = (n_4 L, n_5 L, n_6 L_z)$ , ... The system was checked to make sure that there are no problematically small spacings. We use this system to check the applicability of the anisotropic error formulas for varying shape and inhomogeneity and in the next section to compare the speed of various algorithms.

For the error formulas it is sufficient to consider the standard Ewald summation (**EW3D**). In Fig. 4a the results from a standard Ewald summation are compared to the error formulas Eqs. 13–14. For the reference forces we also used Ewald summation, convergent to 8 digit accuracy in the total energy. The error formulas are satisfactory for both cigar- and pancake-shaped systems (i.e.  $L_z > 1$  and  $L_z < 1$  respectively).

The second concern is the validity of the error formulas when part of the system is empty. This is tested for 10, 50 and 100% filled systems in Fig. 4b. There is no dependence on  $h$  in the error formulas and therefore the error curves should all be the same. In fact there is good agreement and the most substantial deviations occur in the unimportant large- $\alpha$  region. These deviations are evidence of only a small effect of **EW3DLC**-type inhomogeneity on the error

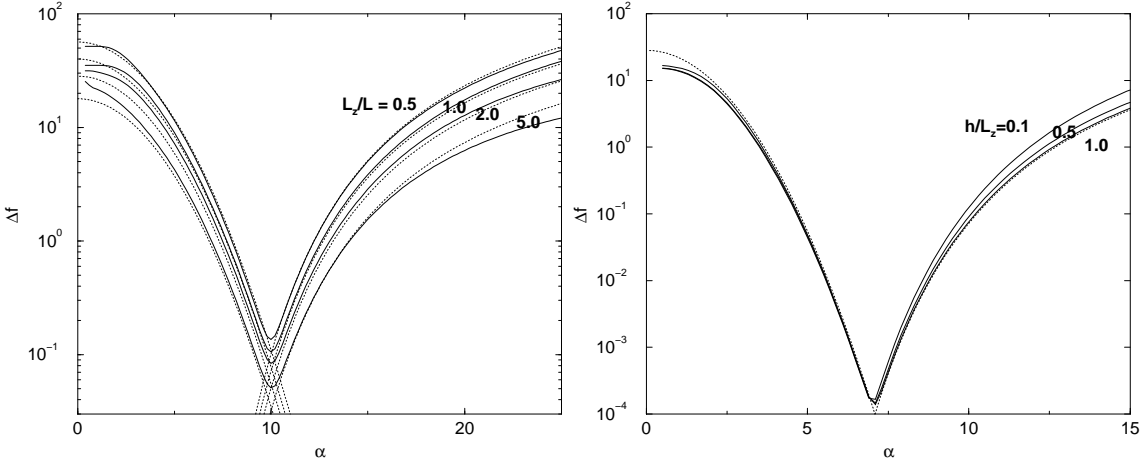


FIG. 4: Dependence of the error estimates on the box shape (a) and the inhomogeneity (b) for standard three-dimensional Ewald summation in a randomized 100 particle system. (a) The aspect ratio  $L_z/L$  of the box is indicated on each curve. The solid lines indicate computations  $(k_c, r_c) = (8, 0.25)$  and the dotted lines are error estimates from Eqns. 13–14. (b) The fill ratio  $h/L_z$  is indicated on each curve. Computations (solid lines) are for  $(8, 0.5)$  and the dotted lines show the error estimates.

formulas.

To summarize, we have shown that the **EW3DLC** method produces accurate and well controlled results and can be used for a broad range of shape and inhomogeneity. This is an important advantage over the **EW3DC** method which is more restrictive on the selection of  $L_z$  even if the error estimate that we developed in the first paper is used to control the error.

## V. COMPUTING TIME

Of course the critical consideration, once issues of accuracy are established, is the speed with which a given algorithm can be implemented. This makes the **P3MLC** the most efficient choice for large  $N$  but for smaller systems other algorithms such as **EW3DLC** or **MMM2D** may have superior speed due to a lower overhead. This section attempts to give some quantitative information on the break-even points between these various algorithms. As usual, the relative times vary slightly with the programming efficiency and the software and hardware of the computer. All times in this study were collected on a Compaq XP1000 workstation.

To optimize the time required for such a many-parameter computation, it is necessary to understand the scaling of time with the variables – most importantly with the number of charges,  $N$ . Here a brief, qualitative discussion of the minimization is made. This discussion tends to be more transparent (with the benefit of hindsight) yet less rigorous than more detailed versions available elsewhere.

The computing time of the real-space part will in general require  $0.5N\rho(4\pi r_c^3/3)$  operations where  $\rho = N/L^2h$  (large  $h$ ) is the density. Similarly the reciprocal-space calculation scales as  $NL_z k_c^3$  since increasing  $L_z$  requires a proportionate increase of the  $z$ -component reciprocal space cutoff. The layer correction scales as  $Nl_c^2$  since it is a cylindrical summation. Thus the overall time required scales as

$$t_{elc} = a_1 N^2 r_c^3 + a_2 N L_z k_c^3 + a_3 N l_c^2 \quad (40)$$

As is evident in plots like Fig. 4, the sharpness of the crossover between the real- and reciprocal-space accuracy regimes is such that the choice of  $\alpha$ ,  $k_c$  and  $r_c$  will be near the optimum if  $\Delta f_r \approx \Delta f_k$ . The layer correction cutoff can be determined independently from the others and moreover is only a weak function of  $L_z$  for large ( $L_z - h$ ). Eq. 40 is then interpreted as a function of two variables, for instance the reciprocal cutoff and the desired accuracy  $t_{elc} = f(k_c, \Delta f)$ . In order to neutralize the change in accuracy in Eqs. 13–14, the Ewald parameter should scale inversely with the real cutoff and linearly with the Fourier cutoff, i.e.  $\alpha \sim 1/r_c \sim k_c$ . Thus we can strike a compromise or balance between the first two terms of Eq. 40 by fixing

$$r_{max} \sim N^{-1/6}, k_{max} \sim N^{1/6} \quad (41)$$

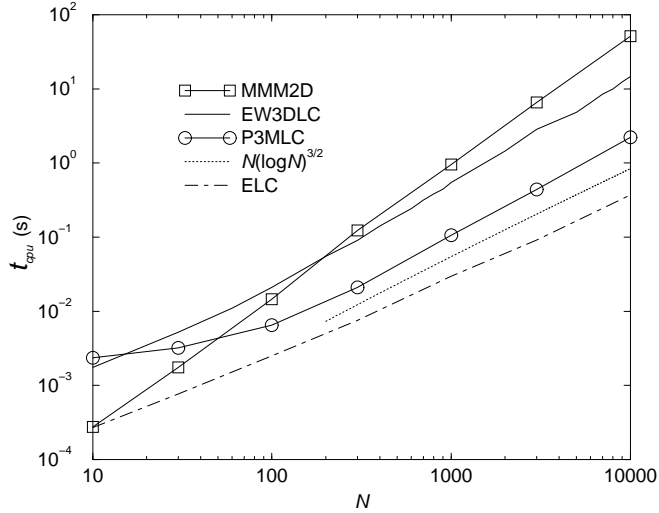


FIG. 5: Optimal CPU times for **P3MLC**, **EW3DLC** and **MMM2D** algorithms. The dotted curve displays the asymptotic scaling of the **P3M** algorithm, and the dot-dashed curve shows the CPU time needed for computing the **ELC**-term.

which reduces the overall scaling of the Ewald calculation to the well-known  $O(N^{3/2})$ . Note that the inclusion of the layer correction does not influence the scaling since it will only add a term linear in  $N$  to Eq. 40. Furthermore, it becomes a smaller part of the overall calculation as  $N$  increases.

A similar analysis applies to mesh-based algorithms, of which we will deal with the **P3M** method. The major difference is that the number of operations required to perform a FFT is independent of the number of charges and only depends on the number of mesh points as  $M \log M$  per direction in space. The other part of the mesh routine is the charge assignment via polynomial interpolation. The order of interpolation,  $P$ , represents the number of grid points in each direction that a given charge is distributed onto. Therefore it is much like a cutoff parameter and the number of operations per charge scales as  $(P + 1)^3$ . The time required for a **P3M** computation is

$$t_{p3mlc} = a_1 N^2 r_c^3 + a_4 L_z (M \log M)^3 + a_5 N (P + 1)^3 + a_3 N l_c^2 \quad (42)$$

An intuitive analysis of Eq. 42 is more difficult but analogous to the preceding reasoning (and benefits from foreknowledge of the answer). Again we attempt to balance the  $N$ -exponent in the first two terms but this time a substantially better result is possible due to the much smaller exponent in the second term (0). From Eq. 15, the choice of  $\alpha \sim M$  will roughly neutralize the effect of  $M$  and thus the link between the mesh size and real cutoff is  $r_c \sim 1/M$ . The best choice for the scaling of these terms is

$$r_c \sim \frac{(\log N)^{1/2}}{N^{1/3}}, M \sim \frac{N^{1/3}}{(\log N)^{1/2}} \quad (43)$$

resulting in an overall scaling for the time of  $O(N(\log N)^{3/2})$ .

The prefactors in the above equations represent a mixture of “primitive” times for various computing operations as well as, for brevity, some unimportant physical parameters. But in general we expect a performance crossover which favors the Ewald method for low  $N$  because of a smaller overhead and eventually at large  $N$ , the **P3M** method becomes much faster.

By generating random systems for a broad range of  $N$  it is possible to obtain an estimate for the crossover. We compare what are perhaps the three best algorithms for slab-like systems in Fig. 5 at a fixed error,  $\Delta f = 10^{-2} e^2 / 4\pi\epsilon L^2$ , including the Coulomb prefactor that has been until now omitted. This level of accuracy is as a value that is practical for Langevin and Brownian dynamics simulations. For instance, in a typical  $N = 3600$ ,  $\rho = 4.2 \cdot 10^{-3}$  polyelectrolyte simulation, the random forces are of order  $2 \cdot 10^3$  times larger than the above RMS electrostatic force error.

The recently introduced non-Ewald **MMM2D** method we recall has a theoretical complexity  $O(N^{5/3})$ . The break-even point between the **MMM2D** and **P3MLC** methods at this low accuracy is approximately  $N^{MMM2D-P3MLC} = 50$  and this would increase monotonically with increasing accuracy. For reference the dotted line in Fig. 5 indicates  $N(\log(N))^{3/2}$  scaling as is expected for the **P3MLC** method. The **EW3DLC** curve plotted shows two break-even

TABLE II: Comparison of **EW3DC** and **EW3DLC**.

system	<b>EW3DLC</b>		<b>EW3DC</b>	
	$(\alpha, r_c, k_c, L_z)$	time (s)	$(\alpha, r_c, k_c, L_z)$	time (s)
pancake	(10.20, 0.271, 9, 0.75)	0.266	(8.30, 0.321, 8, 2.0)	0.342
cube	(8.00, 0.346, 7, 1.5)	0.261	(7.00, 0.384, 7, 3.0)	0.356
cigar	(6.80, 0.410, 6, 2.4)	0.257	(6.90, 0.398, 7, 4.0)	0.368

points at  $N^{MMM2D-EW3DLC} = 200$  and  $N^{EW3DLC-P3MLC} = 17$ . The shape of these curves for the low  $N$  region of the plot is dictated by the computational overhead which can be linear or constant depending on the algorithm. It is necessary to make Verlet lists outside of the timing loop to avoid the quadratic determination of the pair distances in the real-space calculation. Alternatively, these can be subtracted at the end if one accurately measure the primitive time of this step, as we have done. Note also that the layer correction part of the calculation used roughly 20% of the computation time in the scaling regime and the upper bound on its error was fixed at  $10^{-2}$ .

Finally we make a comparison between the speeds of **EW3DLC** and **EW3DC**. Since these methods have the same scaling there is only a difference in the prefactor. But the larger gap size required in **EW3DC** mandates an increase of the reciprocal space cutoff in order to maintain the same accuracy. Thus there is a computational tradeoff between computing the extra layer correction or expanding the region of reciprocal space summation. We have used three systems with different shapes and  $N = 1000$  for the comparison. The first system has a cubic particle volume sized  $1 \times 1 \times 1$  while the other two are pancake and cigar shaped with  $h = 0.5$  and  $2.0$  respectively. The parameters  $(\alpha, r_c, k_c, l_c, L_z)$  were optimized with respect to fixed RMS errors of  $3.0, 4.8$  and  $1.9 \cdot 10^{-2}$  for the pancake, cube and cigar respectively. Again the **ELC** error was chosen conservatively by setting the upper bound to  $10^{-2}$ . These values were chosen in order to compensate for the different volumes of these systems so that the error at the same density is the same for all three shapes.

The results of this analysis are displayed in Table II. Under these conditions, the **EW3DLC** method is only slightly (30%) faster. The reason is that much of the work in these calculations is performed in the real-space and therefore the extra amount of reciprocal-space required by **EW3DC** due to the enlarged gap is not a major issue. In fact it is almost compensated by the time used by layer correction term. For larger  $N$ , **EW3DLC** should become faster than **EW3DC** since the reciprocal-space time becomes much longer than the layer correction time. The same is true about higher accuracy conditions as is observable from the analytical error estimates (Eqs. 13-14). Moreover, in a mesh implementation, the same comparison should yield a more substantial advantage to the layer correction since more of the computational effort is expended in reciprocal space.

## VI. DISCUSSION

We have presented and tested a method with broad applicability and low computational cost for computing the electrostatic forces or energy of a cell of charges with two-dimensional periodicity. This method has a complexity that is virtually linear when applied to a mesh, so that only minor further improvements in computation time can be attempted through a reduction of computational overhead. The algorithm differs from **EW3DC** only by the effort to program the **ELC**-term, but once this is done the errors are easier to control and there is a greater degree of freedom in choosing the box edges. This makes it easy to apply to cubic versions of the **P3M** algorithm (which was one of our initial motivations). For larger systems and better accuracy as may be required in Monte Carlo and some molecular dynamics simulations the method should be considerably faster than **EW3DC**.

It is interesting to estimate the largest system tractable with modern computing. The **P3M** algorithm can be optimized to be at least twice as fast as the version presented here, so an  $N = 10000$  calculation could be carried out in approximately. 2 seconds. A 100-node parallel computer with a 90% scale factor could handle a system of 0.45 million particles in 1 second – which is sufficient for a many molecular dynamics and Monte Carlo simulations.

Finally we can draw attention to several issues suitable for further research. Most importantly we have not treated the case of dissimilar dielectric materials at the slab surfaces. Because of the symmetry of the consequent charge reflections there could be a way to handle the problem efficiently within the current framework. Another topic is the clarification of the dipole term for slab-wise summation for different dielectric constants at the interface between the periodic supersystem and the surroundings.

### Acknowledgments

The authors thank Zuowei Wang and Florian Müller-Plathe for helpful discussions. Financial support from the DFG “Schwerpunkt Polyelektrolyte” is gratefully acknowledged.

### ELC-TERM FORCES AND PRESSURE

For quick reference the force and pressure formulas for the layer correction are given here. The layer correction force on particle  $i$  is

$$\begin{aligned} \mathbf{f}_i^{(lc)} = & -\frac{8\pi}{L_x L_y} \left( \sum_j q_i q_j \left[ 2 \sum_{k_x, k_y > 0} \frac{k_x \cosh(k_{\parallel} z_{ij})}{k_{\parallel} (e^{k_{\parallel} L_z} - 1)} \sin(k_x x_{ij}) \cos(k_y y_{ij}) + \right. \right. \\ & \sum_{k_x > 0} \frac{\cosh(k_x z_{ij})}{(e^{k_x L_z} - 1)} \sin(k_x x_{ij}) \Big], \\ & \sum_j q_i q_j \left[ 2 \sum_{k_x, k_y > 0} \frac{k_y \cosh(k_{\parallel} z_{ij})}{k_{\parallel} (e^{k_{\parallel} L_z} - 1)} \cos(k_x x_{ij}) \sin(k_y y_{ij}) + \right. \\ & \sum_{k_y > 0} \frac{\cosh(k_y z_{ij})}{(e^{k_y L_z} - 1)} \sin(k_y y_{ij}) \Big], \\ & \left. - \sum_j q_i q_j \left[ 2 \sum_{k_x, k_y > 0} \frac{\sinh(k_{\parallel} z_{ij})}{(e^{k_{\parallel} L_z} - 1)} \cos(k_x x_{ij}) \cos(k_y y_{ij}) + \right. \right. \\ & \sum_{k_x > 0} \frac{\sinh(k_x z_{ij})}{(e^{k_x L_z} - 1)} \cos(k_x x_{ij}) + \sum_{k_y > 0} \frac{\sinh(k_y z_{ij})}{(e^{k_y L_z} - 1)} \cos(k_y y_{ij}) \Big] \right). \end{aligned} \quad (44)$$

The diagonal components of the pressure tensor can be obtained from the partition function. For example the normal component is  $P_{\perp} = P_{zz} = -\frac{1}{L_x L_y} \frac{\partial E}{\partial L_z}$ . This yields

$$P_{\perp}^{(lc)} = \frac{8\pi^2}{L_x^2 L_y^2} \sum_{i,j=1}^N q_i q_j \left( 2 \sum_{k_x, k_y \in \mathbb{Z}, > 0} \nu(k_{\parallel}) \cos(k_x x_{ij}) \cos(k_y y_{ij}) + \sum_{k_x > 0} \nu(k_x) \cos(k_x x_{ij}) + \right. \quad (45)$$

$$\left. \sum_{k_y > 0} \nu(k_y) \cos(k_y y_{ij}) \right) \quad (46)$$

where

$$\nu(u) := \frac{(\sinh u z_{ij}) (z_{ij}/L_z) e^{u L_z} - (\sinh u z_{ij}) (z_{ij}/L_z) - (\cosh u z_{ij}) e^{u L_z}}{(e^{u L_z} - 1)^2}. \quad (47)$$

For one of the parallel components we find

$$\begin{aligned} P_{xx}^{(lc)} = & -\frac{8\pi^2}{L_x^2 L_y^2} \sum_{i,j=1}^N q_i q_j \left( 2 \sum_{k_x, k_y \in \mathbb{Z}, > 0} \left[ \frac{k_x^2}{k_{\parallel}^2} \nu(k_{\parallel}) + \frac{k_y^2 \cosh(k_{\parallel} z_{ij})}{k_{\parallel}^3 L_z (e^{k_{\parallel} L_z} - 1)} \right] \cos(k_x x_{ij}) \cos(k_y y_{ij}) + \right. \\ & \sum_{k_x > 0} \nu(k_x) \cos(k_x x_{ij}) + \\ & \left. \sum_{k_y > 0} \frac{1}{k_y L_z} \frac{\cosh(k_y z_{ij})}{(e^{k_y L_z} - 1)} \cos(k_y y_{ij}) \right). \end{aligned} \quad (48)$$

Obviously this is cumbersome since after decomposing the trigonometric and hyperbolic terms to obtain a formula that can be evaluated linearly in  $N$  the expanded version will contain over 80 terms. If rapid pressure calculations are not demanded one can omit this term and increase  $L_z$ . One third of the trace of this tensor will as usual yield the scalar pressure,  $E^{(lc)}/3V$ .

Another consideration in obtaining the pressures is the treatment of the dipole term. Fortunately, a shear or distortion on the system does not result in a distortion in the shape of the supersystem. This is in contrast to the treatment of standard Ewald summation because the spherical summation order requires a complex analysis of the consequences of a distorted sphere.<sup>26</sup>

---

<sup>\*</sup> Electronic address: joannis@mpip-mainz.mpg.de  
<sup>†</sup> Electronic address: arnolda@mpip-mainz.mpg.de  
<sup>‡</sup> Electronic address: holm@mpip-mainz.mpg.de

<sup>1</sup> A. H. Widmann and D. B. Adolf, *Comp. Phys. Comm.* **107**, 167 (1997).  
<sup>2</sup> D. Parry, *Surf. Sci.* **49**, 433 (1975).  
<sup>3</sup> D. E. Parry, *Surf. Sci.* **54**, 195 (1976).  
<sup>4</sup> D. M. Heyes, M. Barber, and J. H. R. Clarke, *J. Chem. Soc. Faraday Trans. II* **73**, 1485 (1977).  
<sup>5</sup> S. W. de Leeuw and J. W. Perram, *Physica* **113A**, 546 (1982).  
<sup>6</sup> M. Porto, *J. Phys. A* **33**, 6211 (2000).  
<sup>7</sup> R. Strelbel and R. Sperb, *Molecular Simulation* **27**, 61 (2001).  
<sup>8</sup> A. Arnold and C. Holm, *Chem. Phys. Lett.*, in press, and preprint cond-mat/0202265.  
<sup>9</sup> Technically this space is not “empty” rather, it is filled with a solvent of the same dielectric constant.  
<sup>10</sup> E. Spohr, *J. Chem. Phys.* **107**, 6342 (1997).  
<sup>11</sup> S. W. de Leeuw, J. W. Perram, and E. R. Smith, *Proc. R. Soc. Lond. A* **373**, 27 (1980).  
<sup>12</sup> S. W. de Leeuw, J. W. Perram, and E. R. Smith, *Proc. R. Soc. Lond. A* **373**, 57 (1980).  
<sup>13</sup> I.-C. Yeh and M. L. Berkowitz, *J. Chem. Phys.* **111**, 3155 (1999).  
<sup>14</sup> E. R. Smith, *Proc. R. Soc. Lond. A* **375**, 475 (1981).  
<sup>15</sup> A. Arnold, J. de Joannis, and C. Holm, **submitted** (2002), preprint cond-mat/0202399.  
<sup>16</sup> L. Greengard and V. Rhoklin, *J. Comp. Phys.* **73**, 325 (1987).  
<sup>17</sup> K. Esselink, *Comp. Phys. Comm.* **87**, 375 (1995).  
<sup>18</sup> J. Lekner, *Physica A* **176**, 485 (1991).  
<sup>19</sup> P. Ewald, *Ann. Phys.* **64**, 253 (1921).  
<sup>20</sup> R. W. Hockney and J. W. Eastwood, *Computer Simulation Using Particles*, IOP, London, 1988.  
<sup>21</sup> The summation order of the layer correction is implicitly cylindrical. It probably does not matter whether the summation proceeds along the radius of the cylinder first and then along its axis (as written) or vice versa. But they may not proceed simultaneously.  
<sup>22</sup> J. Kolafa and J. W. Perram, *Molecular Simulation* **9**, 351 (1992).  
<sup>23</sup> H. G. Petersen, *J. Chem. Phys.* **103**, 3668 (1995).  
<sup>24</sup> M. Deserno and C. Holm, *J. Chem. Phys.* **109**, 7694 (1998).  
<sup>25</sup> M. Deserno and C. Holm, *J. Chem. Phys.* **109**, 7678 (1998).  
<sup>26</sup> E. R. Smith, *J. Stat. Phys.* **77**, 449 (1994).